Duct System of the Rabbit Lacrimal Gland: Structural Characteristics and Role in Lacrimal Secretion

Chuanqing Ding,[1] *Leili Parsa,*[1,2] *Prachi Nandoskar,*[1] *Ping Zhao,*[3] *Kaijin Wu,*[4] *and Yanru Wang*[5]

Purpose. To develop a nomenclature for the lacrimal duct system in the rabbit, based on the anatomic and structural characteristics of each duct segment, and to provide RT-PCR and immunofluorescence data to support the notion that the duct system plays important roles in lacrimal function.

Methods. Paraffin-embedded lacrimal glands (LGs) were stained with hematoxylin and eosin (H&E) and evaluated with a stereomicroscope. Cryosections of LG were stained with cresyl violet, and acinar cells and ductal epithelial cells were isolated from each duct segment by laser capture microdissection (LCM). mRNA levels from these cells were analyzed by real-time RT-PCR. Standard protocol was followed for immunofluorescence detection of ionic transporters.

Results. The lacrimal duct system was divided into six segments on the basis of morphologic characteristics: the intercalated, intralobular, interlobular, intralobar, interlobar, and main excretory ducts. Although the morphologic features change incrementally along the entire duct system, the gene expression of ionic transporters and aquaporins, including AE3, AQP4, AQP5, CFTR, ClC2γ, KCC1, NHE1, NKAα1, NKAβ1, NKAβ2, NKAβ3, and NKCC1 varied greatly among duct segments. Immunofluorescence results were generally in accordance with the abundance of mRNAs along the acinus–duct axis.

Conclusions. Most LG research has focused on the acinar cells, with relatively little attention being paid to the lacrimal ducts. The lack of knowledge regarding the lacrimal ducts was so profound that a precise nomenclature had not been established for the duct system. The present data establish a nomenclature for each segment of the lacrimal duct system and provide evidence that ducts play critical roles in lacrimal secretion. (*Invest Ophthalmol Vis Sci.* 2010;51:2960–2967) DOI:10.1167/iovs.09-4687

From the Departments of [1]Cell and Neurobiology, [4]Pharmacology and Pharmaceutical Sciences, and [5]Physiology and Biophysics, University of Southern California, Los Angeles, California; and the [3]Department of Ophthalmology, Third Hospital of Hebei Medical University, Shijiazhuang, Hebei, China.

[2]Present affiliation: private practice in Baltimore, Maryland.

Supported by NIH Grants EY017731 (CD), EY10550 (JES), EY05801 (AKM), P30 DK048522 (Core Facilities of the USC Research Center for Liver Diseases), and EY03040 (Doheny Eye Institute Core).

Submitted for publication September 24, 2009; revised January 8, 2010; accepted January 16, 2010.

Disclosure: **C. Ding**, None; **L. Parsa**, None; **P. Nandoskar**, None; **P. Zhao**, None; **K. Wu**, None; **Y. Wang**, None

Corresponding author: Chuanqing Ding, Department of Cell and Neurobiology, University of Southern California, Keck School of Medicine, 1333 San Pablo Street, BMT 304, Los Angeles, CA 90089-9112; cding@usc.edu.

Dry eye syndrome afflicts millions of Americans. It often results from insufficient formation of fluid in the lacrimal gland (LG). It has been thought that primary lacrimal fluid is formed in the acini and then is modified during passage through the lacrimal duct system to the ocular surface. Ductal cells have been estimated to account for ~15% of the total mass of the LG.[1–3] A review of the literature reveals very few studies of the LG duct system, in striking contrast to a wealth of information that has been gained on duct systems of the salivary glands and pancreas, which are structurally and functionally homologous to the LGs.[4,5]

In salivary glands, the duct system has been divided into several segments based on its structural characteristics and functional relevance to gland secretion. The duct segments are most commonly referred to as the intercalated, striated, intralobular, interlobular, intralobar, interlobar, and main excretory segments. However, the duct system in the LG has not been well characterized.

Like the salivary glands, LGs are composed of several large lobes that are divided into smaller lobules composed of numerous secretory end pieces, the acini. The duct system is also highly branched (Fig. 1) and is responsible for transporting lacrimal fluids to the ocular surface. Our recent findings have suggested that the lacrimal duct system can also be divided into various segments based on their anatomic and structural characteristics and the duct segments most likely play distinctive functions in monitoring and altering the luminal content as it flows toward the ocular surface. We have therefore formulated a nomenclature for the lacrimal duct system, largely in accordance with that of salivary glands, with no striated duct being observed in LG (see the Results section for details). We also analyzed the gene expression patterns in various duct segments and the acini. Immunofluorescence detection of the proteins translated from these genes was also performed to verify their expression pattern within the LG. Taken together, our data showed the diverse structural characteristics of lacrimal ducts and suggest possible functional differences among specific duct segments in lacrimal fluid production.

Materials and Methods

Animals

Six adult female New Zealand White rabbits (Irish Farms, Norco, CA) weighing approximately 4.0 kg were used. The animals were narcotized with a mixture of ketamine (40 mg/mL) and xylazine (10 mg/mL) and given an overdose of pentobarbital (80 mg/kg) for euthanatization. This study conformed to the standards and procedures for the proper care and use of animals as described in the ARVO Statement for the Use of Animals in Ophthalmic Research.

Histology

Inferior LGs were fixed in 10% formalin and embedded in paraffin. Tissue blocks were sectioned at 5 μm, deparaffinized, and stained with

Copyright © Association for Research in Vision and Ophthalmology

Downloaded from iovs.arvojournals.org on 04/23/2024

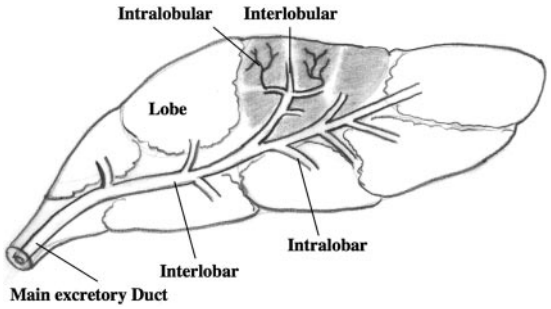

FIGURE 1. Illustration of the lacrimal duct system. The LG is composed of several lobes, which are further subdivided into lobules (shown in the *shaded* lobe). The lacrimal duct system is a tree-like structure and, on the basis of its anatomic and structural characteristics, it can be divided into, from the acini to the ocular surface: intralobular, interlobular, intralobar, interlobar, and main excretory ducts. Illustration courtesy of Joel Schechter, PhD.

hematoxylin and eosin (H&E). The slides were examined with a microscope (Eclipse 80i; Nikon, Tokyo, Japan) equipped with a digital camera (Optronics, Goleta, CA), and images were captured (PictureFrame; Optronics).

Laser Capture Microdissection

The inferior LGs were removed in RNase-free conditions, placed in OCT (Miles, Elkart, IN), and rapidly frozen with liquid nitrogen. The frozen sections were collected with membrane-coated slides (PEN; Leica Microsystems, Deerfield, IL) and stained with cresyl violet in RNase-free conditions (LCM Staining Kit; Applied Biosystems, Inc. [ABI], Foster City, CA), according to the manufacturer's protocol. Tissue sections were then laser captured (PixCell II LCM System; Arcturus Bioscience, Mountain View, CA). All microdissections were performed using with laser capture microdissection (LCM) caps (CapSure HS; Molecular Devices, Sunnyvale, CA) under RNase-free conditions. Approximately 100 cells were collected from each acinus and duct segment sample for isolation of total mRNA, and six replicates of each acinus and duct segment were collected from each animal.

RNA Extraction and Reverse Transcription

Total cellular RNA was isolated from RNA stabilizer–treated tissue samples (RNALater and RNAqueous Micro kit; Ambion, Austin, TX) according to the manufacturer's protocol, which was optimized for LCM samples. RNA was eluted twice from a silica-based microfilter cartridge with an 11-μL volume of prewarmed (95°C) elution solution. RNA samples were then treated with DNase I to degrade any potential contaminating DNA. RNA quality and quantity were evaluated with a spectrophotometer (ND-1000; Nanodrop Technologies, Wilmington, DE). The RNA samples were then reverse-transcribed to cDNA only if the 260/280 ratio was above 1.9 (High Capacity cDNA Reverse Transcription Kit with RNase Inhibitor; ABI). Each RT reaction contained 20 μL of total RNA, 4 μL of 10× RT buffer, 1.6 μL of 25× dNTP mixture, 4 μL of 10× random primers, 2 μL reverse transcriptase (50 U/μL; MultiScribe RT; ABI), 2 μL RNase inhibitor, and 6.4 μL of RNase-free water. The 40-μL reactions were incubated in a thermal cycler (DNA Engine; Bio-Rad, Hercules, CA) for 10 minutes at 25°C, 2 hours at 37°C, and 5 seconds at 85°C and then stored at 4°C.

Real-Time RT-PCR with Pre-amplification

The preamplification was performed with commercial master mix (TaqMan PreAmp Master Mix Kit; ABI). The pooled assay mix was prepared by combining up to 50 of 20× gene expression assays (TaqMan; ABI) into a single tube and using nuclease-free water to dilute the pooled assays to a final concentration of 0.2×. The 50 μL of preamplification reaction included 25 μL of 2× mastermix (PreAmp Master Mix, TaqMan; ABI) 12.5 μL of 0.2× pooled assay mix and 12.5 μL of cDNA sample. The reactions were incubated in the thermal cycler for 10 minutes at 95°C followed by 14 cycles at 95°C for 15 seconds and 4 minutes at 60°C and then held at 4°C. The preamplification product was then 1:20 diluted with 1× TE buffer and analyzed by real-time RT-PCR (TaqMan; ABI).

The sequences of the primers and probes used in this study are listed in Table 1. The sequences were selected on computer (Primer Express; ABI) and synthesized by ABI. All probes incorporated the 5′ reporter dye 6-carboxyfluorescin (FAM) and the 3′ quencher dye 6-carboxytertramethylrhodamine (TAMRA).

For the real-time RT-PCR step, amplification was performed on a sequence-detection system (Prism 7900HT, with TaqMan Gene Expression Master Mix; ABI) containing the internal dye ROX as a passive reference, in accordance with the procedures described. The PCR reaction volume was 10 μL. It contained 1× master mix, 900 nM forward and reverse primers, 250 nM probes, and 2.5 μL of 1× TE– diluted cDNA template. The FAM signal was measured against the ROX signal to normalize for non-PCR-related fluorescence fluctuations. The cycle threshold (C_T) value represented the refraction cycle number at which a positive amplification reaction was measured and was set at 10× the standard deviation from the mean baseline emission calculated for PCR cycles 3 through 15. Each sample was measured in triplicate. The difference between the C_T for each target mRNA and the internal housekeeping gene *GAPDH* in each sample was used to calculate the level of target mRNA relative to that of *GAPDH* mRNA in the same sample.[6]

Immunofluorescence

Standard protocol was followed for immunofluorescence experiments. The antibodies used were goat anti-AQP4 (C-19) polyclonal antibody (Santa Cruz Biotechnology, Santa Cruz, CA), at a dilution of 1:50; goat anti-AQP5 (C-19) polyclonal antibody (Santa Cruz), dilution 1:400; goat anti-NKCC1 (N-16) polyclonal antibody (Santa Cruz), dilution 1:50; mouse anti-NKA β1 (C464.8) monoclonal antibody (Santa Cruz), dilution 1:100; mouse anti-NHE1 (C terminus, clone 4E9) monoclonal antibody (Millipore, Temecula, CA), dilution 1:100; mouse anti-CFTR (C terminus) monoclonal antibody (R&D Systems, Minneapolis, MN), dilution 1:250; and mouse anti-ClC2γ monoclonal antibody (Abcam, Cambridge, MA), dilution 1:100. The secondary antibodies used were fluorescein isothiocyanate (FITC)– or rhodamine red–conjugated donkey IgG, dilution 1:400 (Jackson ImmunoResearch, West Grove, PA). Rhodamine-conjugated phalloidin (Invitrogen, Carlsbad, CA), at a dilution of 1:200, was also used on some slides to stain F-actin. Slides were examined with a laser scanning confocal microscope (LSM510; Carl Zeiss Meditec, Dublin, CA) and the images analyzed with image-editing software (PhotoShop; Adobe Systems, Mountain View, CA).

RESULTS

Morphologic Characteristics and Nomenclature of Duct Segments

The smallest branches of the duct system are the intercalated ducts, to which the secretory end pieces are attached and emerge from the acini as a distinctive group of cells. These ducts are composed of a single layer of cuboidal cells that stain red (eosinophilic) in a smooth pattern, in contrast to the pyramid-shaped acinar cells that typically show a foamy and pale appearance because of the numerous glycoprotein-rich secretory granules in the cytoplasm (Fig. 2A). Several intercalated ducts merge into larger intralobular ducts. The epithelial cells in the intralobular ducts are also cuboidal in shape and are stained slightly deeper than intercalated ductal cells. Both intercalated and intralobular ducts are in immediate continuity with acini and are surrounded by minimal loose connective tissue. Intercellular plasma membranes are not as easily identified as those between acinar cells. The nuclei in the interca-

Downloaded from iovs.arvojournals.org on 04/23/2024

TABLE 1. Primers and Probes Used for Real-Time RT-PCR

Gene	Forward Primer	Reverse Primer	Probe	Accession No.
AE3	5′-ATTTCGGCATCCCCATCTC-3′	5′-CAACTTCTGAGTGTAGGTGTCTGTGA-3′	5′-CTGCTGATGGTCTTGGTGATTAC-3′	AF031650
AQP4	5′-CGTTTTAAAGAAGCCTTCAGCAA-3′	5′-CCTGTTGTCCTCCACCTCCAT-3′	5′-CTGCCCAGCAAACGAAAGGAGCTA-3′	AF000312
AQP5	5′-GGGCAACGTGGCTGTCAA-3′	5′-AGCTGGAAGGTGAGGATCAACTC-3′	5′-CTCAACGAACAACACGACACCGGGC-3′	AF495879
CFTR	5′-GGGCTGCTCTGGGAACTACTAC-3′	5′-CCTAGCCCGGCTTGAACAA-3′	5′-TTCTGCGGCCTTGCTTTCCTAATAGTCC-3′	AF189720
ClC2g	5′-CATCGGAGGCGTCCTATTCA-3′	5′-AAGCCGCGCCAGTAGTTG-3′	5′-AGGTCACCTCCACCTTCTTCGC-3′	U15652
ENaCa	5′-GGTGCACGGACAGGATGAG-3′	5′-CCGGGCCGCAAGTTAAA-3′	5′-CTGCCTTTATGGATGATGGCG-3′	AF229025
ENaCg	5′-TCCATCGGCAGGACGAATA-3′	5′-ACATGGCCGTCTCGATCTCT-3′	5′-CCCTTCATTGAAGATGTGGGCA-3′	AF229027
KCCl	5′-CCCGCCTGGTCCTACTGA-3′	5′-AGTTCTCATCACCCTCGCTGTT-3′	5′-CATGCCCGGCCCACCCAA-3′	U55053
NHE1	5′-GCCTTCACCTCCCGATTCA-3′	5′-AGGCCATGTAGCTGTAGAGGAAGA-3′	5′-CGCGTCATCGAGCGCGCTCT-3′	X61504
NKAa1	5′-GCTGTCCATTCATAAGAACCTCAA-3′	5′-TCTGGAGCGCCCTTCATC-3′	5′-CAATGAGCCACGGCACCTGCTAG-3′	AF235024
NKAa2	5′-TCGGGACGGACCCAATG-3′	5′-AAGCTGGCGACAGAACTTGAC-3′	5′-CCTCACTCCACCCCCGACAACTCC-3′	AF235025
NKAb1	5′-GCCCAGAAGGATGACATGGT-3′	5′-CGCCTCGTTCTTTAGGTTCACT-3′	5′-TTGAAGATTGTGGCGACGTGC-3′	AF204927
NKAb2	5′-GCCCCGGGCGCTATT-3′	5′-AGCGCGTTTCGGGTAGTTG-3′	5′-CGAACAGCCGGATAACGGAGTCC-3′	AY069937
NKAb3	5′-TGCTTCAAGCATGCAGTGGTA-3′	5′-CACAAGAACACAAGGGCTTCCT-3′	5′-AGTGATCGTGATTTTGGCTATTCC-3′	AF302929
NKCC1	5′-GGTGCGATTGGCCTGATC-3′	5′-ATCCCACCACATACATAGCAACTG-3′	5′-TTGCTTTTGCCAACGCTGTT-3′	AF170447

FIGURE 2. Segments of the lacrimal duct system. (**A**) Intercalated ducts (*arrow*) emerge from acini and merge into larger intralobular duct (*arrowhead*). Cells of intercalated ducts are simple cuboidal and stain *red* with H&E. The intracellular contents appear smooth, rather than the pale and foamy appearance of acinar cells. Several intercalated ducts merge into larger intralobular ducts that have much larger lumens. Intercalated and intralobular ducts drain acini and are in immediate continuity with acini and have minimal connective tissues surrounding them. OD ranges from 20 to 30 μm. An intralobar duct can be seen in the upper right corner. Ac, acinus. (**B**) Interlobular ducts (*arrow*) are merged from intralobular ducts (~30 to 50 μm OD). Duct cells range from simple cuboidal to low columnar and stain *red* with a smooth appearance of intracellular contents. These ducts drain lobules, having connective tissue, and frequently, blood vessels surrounding them. Two intralobular ducts are also visible in this image (*arrowheads*). (**C**) Intralobar ducts (*arrow*) drain individual lobes. Duct cells are low to tall columnar and range from simple to pseudostratified epithelial cells. These ducts are surrounded by increasingly more connective tissues and often with blood vessels (~50 to 80 μm OD). Note that an intralobular duct (*arrowhead*) can be seen with a small lumen and in immediate continuity with acini. (**D**) Interlobar ducts (*arrow*) are merged from intralobar ducts. Ducts range from simple to stratified columnar epithelia, ~80 to 200 μm OD, albeit the luminal profiles are highly variable. These duct segments are surrounded by abundant connective tissue. Scale bar, 100 μm.

lated and intralobular duct cells are slightly bigger than those in acinar cells and appear more spherical in shape (Fig. 2).

Structures equivalent to the striated ducts present in salivary glands could not be identified in the H&E sections of the LGs. In salivary glands, the striated ducts emerge from intercalated ducts and flow into larger intralobular ducts. Their striated appearance is caused by closely packed, mitochondria-lined infoldings of the epithelial cell basolateral membranes. The distinctive basal membranes in striated ducts have numerous mitochondria between basal infoldings that give them a striated appearance and greatly extend the area of membrane available for exchange of water and ions in a fashion similar to that of the proximal convoluted tubule of the kidney. Because striated ducts are absent in the LGs, we therefore grouped the intercalated ducts together with the intralobular ducts in the LCM and RT-PCR studies. The outer diameter (OD) of the intercalated and intralobular ducts ranges from 20 to 30 μm.

Intralobular ducts merge into interlobular ducts, which drain several lobules. Interlobular duct cells range from simple

Downloaded from iovs.arvojournals.org on 04/23/2024

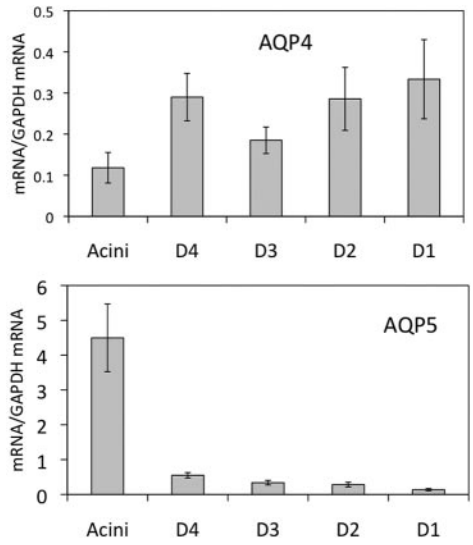

FIGURE 3. Real-time RT-PCR of AQPs. The level of AQP4 mRNA was the lowest in the acini, but increased significantly in the intralobular, intralobar, and interlobar ducts. The expression of AQP4 mRNA was also significantly higher in intralobular ducts than in interlobular ones. AQP5 mRNA levels showed a completely different pattern. It was nine times higher in the acini than in the intralobular ducts and three times higher in the intralobular than in the interlobar ducts. Moreover, although AQP5 mRNA was 40 times more abundant than AQP4 mRNA in the acini, the two transcripts were at similar levels in the intralobular ducts. D4, intralobular duct; D3, interlobular duct; D2, intralobar duct; D1, interlobar duct. Data are presented as the mean ± SEM.

cuboidal to low columnar. They stain deeply with eosin without distinctive intercellular plasma membranes visible between duct cells, and the intracellular contents appear smooth rather than having the pale cotton-wool pattern observed in acinar cells. Nuclei in these ducts are spherical and are located close to the basal membrane. The OD of the interlobular ducts ranges from 30 to 50 μm. They are generally surrounded by loose connective tissue and are often accompanied by neurovascular bundles (Fig. 2B).

Interlobular ducts merge into intralobar ducts, which drain individual lobes. Epithelial cells that constitute the intralobar ducts are short-to-tall columnar cells and range from simple to pseudostratified. Their nuclei are spherical and located close to the basal membrane. Their OD ranges from 50 to 80 μm. They are surrounded by increasingly more connective tissue and, like interlobular ducts, are often accompanied by neurovascular bundles (Fig. 2C).

Interlobar ducts are of variable dimensions due to compression by surrounding tissue (i.e., sometimes with highly folded luminal contours) and are surrounded by increasingly more connective tissue and neurovascular bundles. The epithelial cells range from simple to pseudostratified and stratified columnar, and the number of cell layers increases as they approach the main excretory duct. OD ranges from 80 to 200 μm (Fig. 2D).

Expression of Transport Protein mRNAs

Aquaporins are the membrane proteins that are responsible for fast water transport across plasma membranes. The direction in which the water flows is determined by osmotic gradients, which largely are established through the actions of various ion transport proteins. The abundance of mRNAs for aquaporins and ion transport proteins varied significantly among acini and different duct segments.

As illustrated in Figure 3, AQP4 mRNA was significantly more abundant in the intralobular, intralobar, and interlobar ducts than in the acini. It also was significantly more abundant in the intralobular ducts than in the interlobular ones. The level of AQP5 mRNA showed a completely different pattern. It was nine times higher in acini than in the intralobular ducts and three times higher in the intralobular than in the interlobar ducts. Moreover, although AQP5 mRNA was 40 times more abundant than AQP4 mRNA in acini, the two transcripts were at similar levels in the intralobular ducts.

Na^+/K^+-ATPase (NKA), an enzyme located in the plasma membrane in all animals, is composed of α and β subunits, and although two isoforms of the α subunit (α1 and α2) and three isoforms of β subunit (β1, β2, and β3) have been identified so far, we were unable to detect significant amount of α2 in our samples. As shown in Figure 4, NKAα1 mRNA was significantly more abundant in intralobular ducts than in acini. NKAβ1 mRNA was similarly expressed in intralobular ducts and acini, but less so in interlobular ducts. Significant levels of NKAβ2 mRNA were detected in interlobular and interlobar ducts, but not in acini and intralobular ducts. NKAβ3 mRNA was significantly more abundant in intralobular ducts than in acini and the other duct segments.

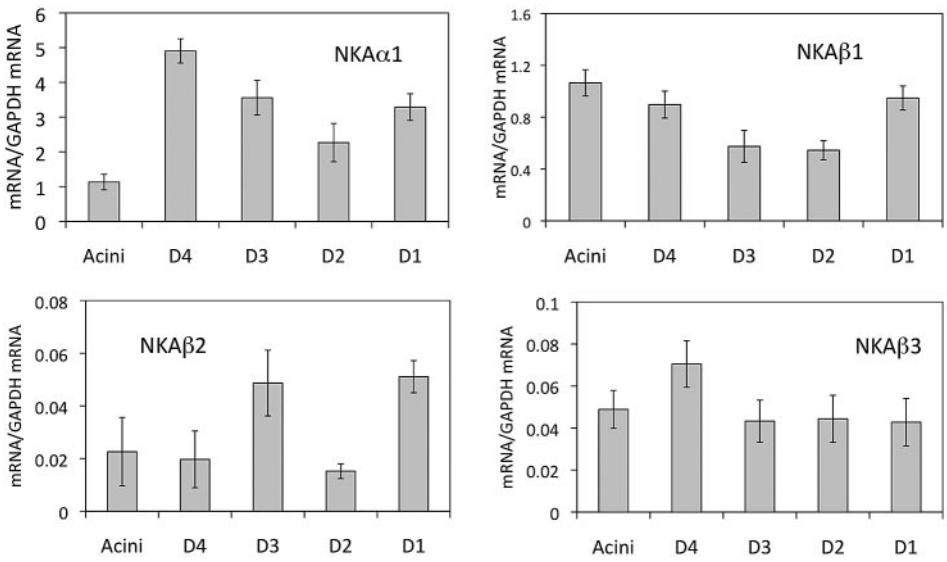

FIGURE 4. Real-time RT-PCR of Na^+/K^+-ATPase (NKA) subunits. α1 mRNA was the least abundant in acini, whereas its level in the intralobular ducts was significantly more higher. β1 mRNA was similarly present in intralobular ducts and acini, but less so in interlobular ducts. Significant levels of NKAβ2 mRNA were detected in the interlobular and interlobar ducts, but not in the acini and intralobular ducts. NKAβ3 mRNA was significantly more abundant in the intralobular ducts than in the acini and the other duct segments. We were unable to detect a meaningful presence of α2. Labeling and data are as in Figure 3.

Downloaded from iovs.arvojournals.org on 04/23/2024

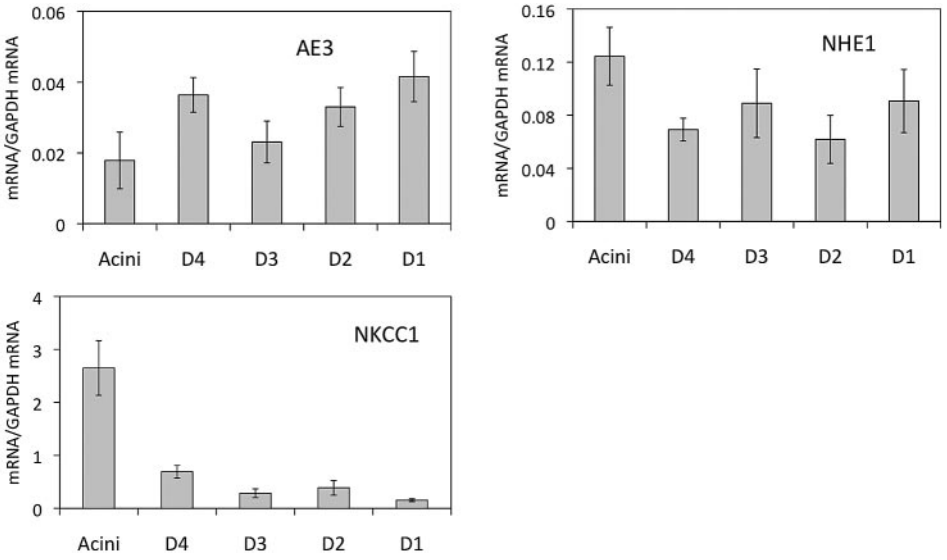

FIGURE 5. Real-time RT-PCR of transporters involved in Na^+-Cl^--coupled entry mechanisms. The level of AE3 mRNA was the lowest in acini and significantly increased in intralobular, intralobar, and interlobar ducts. NHE1 and NKCC1 showed a similar pattern of mRNA expression in acini and duct segments (i.e., the highest was found in acini, whereas the duct segments had less mRNA, although the difference between expression in acini and duct segments was much more dramatic for NKCC1). Labeling and data are as in Figure 3.

The anion exchanger (AE) mediates Cl^-/HCO_3^- exchange as well as Cl^-/Cl^- exchange and HCO_3^-/HCO_3^- self-exchange. Three isoforms of AE have been identified so far (AE1, AE2, AE3). The Na^+/H^+ exchangers, designated NHE, mediate the corresponding cation exchanges. The $Na^+/K^+/2Cl^-$ cotransporter, designated NKCC, obligatorily couple fluxes of the three ions through plasma membranes. As shown in Figure 5, mRNAs for NKCC1 and NHE1 were more abundant in acini than in the ducts. In contrast, significant levels of AE3 mRNA were detected in the ducts but not in the acini. Note also the substantial difference in the relative abundance of the mRNAs of the three transport proteins.

K^+2Cl^- cotransporters (KCCs) mediate obligatorily coupled fluxes of K^+ and Cl^- through cell membranes. Significant levels of KCC1 mRNA were detected in intralobular, intralobar, and interlobar ducts, but not in acini or interlobular ducts (Fig. 6).

The cystic fibrosis transport regulator (CFTR) functions as a Cl^--selective channel that can mediate either influx or efflux, depending on the orientation of the Cl^- electrochemical potential gradient. Significant levels of CFTR mRNA were detected in intra- and interlobular ducts and in intra- and interlobar ducts, but not in acini (Fig. 7). ClC is another membrane transport protein that is responsible for transporting chloride across plasma membranes. PCR studies showed that the mRNA of ClC2γ was significantly higher in acini and interlobular ducts than in other duct segments.

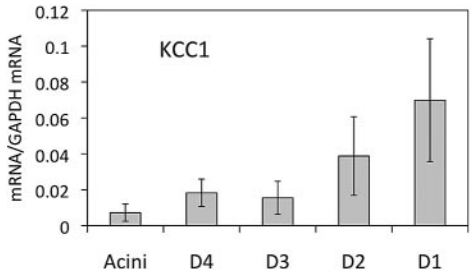

FIGURE 6. Real-time RT-PCR of K-$2Cl^-$, which is involved in a coupled efflux mechanism. KCC1 is responsible for the efflux of Cl^- and K^+ across the basolateral membranes in LG epithelial cells. The level of mRNA was the lowest in acini, and its abundance increased significantly in intralobular, intralobar, and interlobar ducts. Labeling and data are as in Figure 3.

Immunofluorescence

Immunofluorescence results indicated that distributions of AQP and transporter immunoreactivity (IR) was generally in accordance with the abundance of mRNAs along the acinus-duct axis.

AQP4-IR was found on the basolateral sides of the acinar and ductal cells, with ductal cells showing stronger AQP4-IR than acinar cells (Fig. 8A). However, the smooth, thick, undulating pattern of AQP4-IR also suggests that some of the IRs were on the myoepithelial cells. AQP5-IR was found in all acinar cells, but was distributed among the acini in a mosaic pattern, with some acini and/or acinar cells demonstrating much stronger AQP5-IR than others. However, virtually no AQP5-IR was detected in duct cells (Fig. 8B).

NKAβ_1-IR was present in all acinar cells, but, like AQP5-IR, levels differed in a mosaic pattern, higher in some acinar cells and/or acini than in others. However, contrary to AQP5-IR, NKAβ_1-IR in ductal cells was uniformly high (Fig. 8C).

NHE1-IR was found at the basolateral membranes and within the cytoplasm of all acinar and ductal cells, but the level in ductal cells was considerably higher (Fig. 8D). NKCC1-IR was also present on the basolateral membranes and within the cytoplasm of all acinar and ductal cells, but, contrary to NHE1-IR, the levels of NKCC1-IR were higher in the acinar cells (Fig. 8E).

Both CFTR-IR and ClC2γ-IR were weakly detected in the LGs. CFTR-IR was present in punctate aggregates within the apical cytoplasm of all acinar and ductal cells, but the level in the ductal cells was considerably higher (Fig. 8F). The strongest CFTR-IR was found in intra- and interlobular ducts, compared with that in intra- and interlobar ducts. Rhodamine-conjugated phalloidin, which stains F-actin, was used to outline the morphologic profile. Like CFTR, ClC2γ-IR was also found in the apical cytoplasm as punctate aggregates. However, no ClC2γ-IR was seen in the ductal cells (Fig. 8G).

DISCUSSION

The importance of the tear film and its role as an indispensable integral component of the ocular surface system is well established.[7] Although dry eye syndrome afflicts millions of people, the underlying etiology remains unknown, and our understanding of the normal physiology of the LG is still far from com-

Downloaded from iovs.arvojournals.org on 04/23/2024

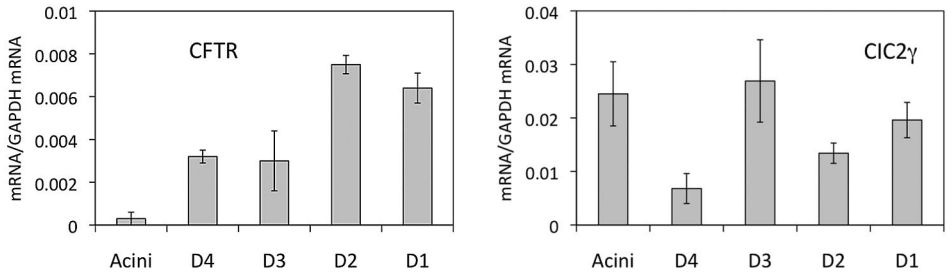

FIGURE 7. CFTR and ClCγ mRNA levels in acini and duct segments. Both transporters are membrane channels that transport chloride across plasma membranes. Minimal CFTR mRNA was found in acini, whereas its level was significantly higher in every duct segment, with the highest observed in the interlobar duct. The expression of ClC2γ mRNA was the lowest in the intralobular duct, whereas the acini and interlobular duct had significantly higher levels. Labeling and data are as in Figure 3.

plete. To date, almost all studies of LG function have focused on the acinar cells, and only a few have focused on the duct system, which has been estimated to represent ~15% of all the epithelial cells within the LG.[8,9]

Although investigators have used various terminologies for the LG duct segments[10–19] (e.g., intercalated duct, intralobular duct, and interlobular duct), we were unable to find literature that focused on characterizing each specific duct segment. In fact researchers in many publications simply referred to "ducts" without clarifying which segment they meant.

In the present study we established a nomenclature for the lacrimal duct system in the rabbit and demonstrated the structural characteristics of each duct segment. In general, this system was in accordance with that in the salivary gland, an exocrine gland that has received much more extensive research with respect to the features and functions of ductal segments. In the rabbit LG, we were unable to identify striated ducts comparable to those described in the salivary gland. Striated ducts are a transitional segment between intercalated ducts and the remaining larger intralobular ducts in the salivary

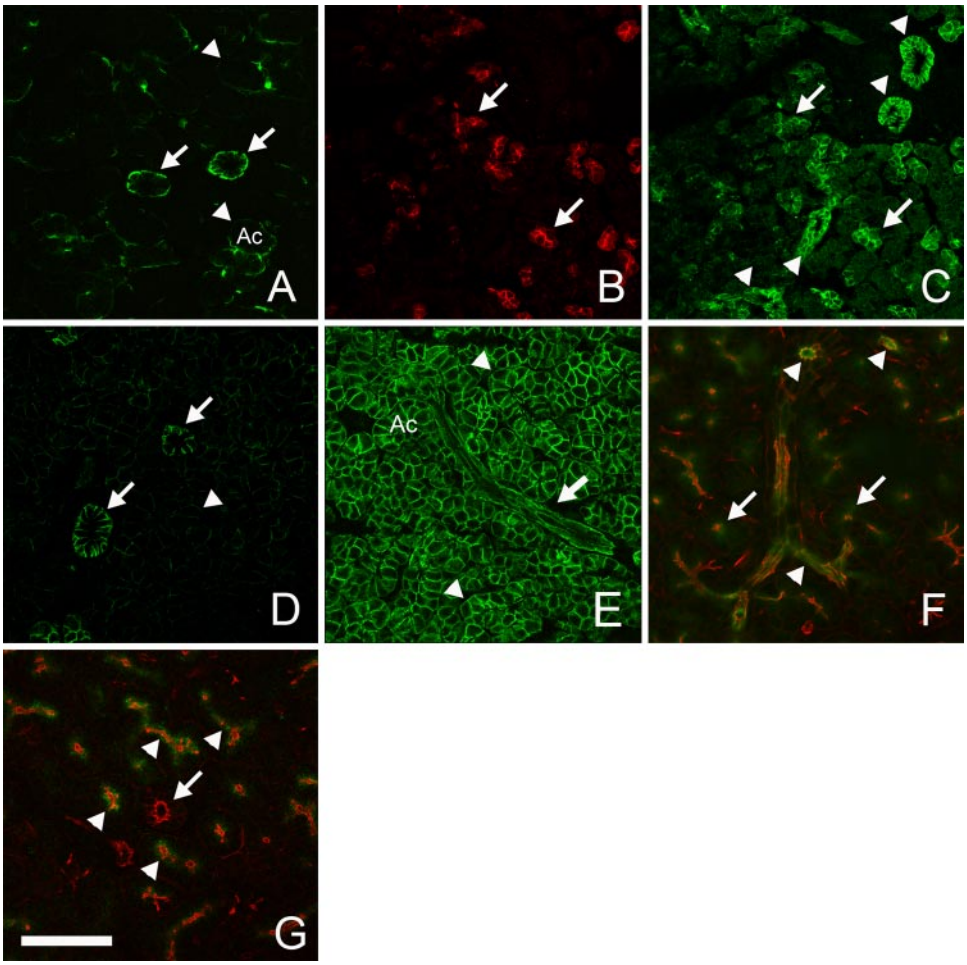

FIGURE 8. Immunofluorescence of AQPs and transporters. (**A**) AQP4-IR was observed on the basolateral sides of acinar and duct cells, with duct cells (*arrows*) showing a stronger IR than acinar cells (*arrowheads*). (**B**) AQP5-IR was distributed among acini in a mosaic pattern, with some acini and/or acinar cells demonstrating much stronger IR (*arrows*) than the rest of the acini/acinar cells. However, virtually no IR was detected in duct cells (**C**, *arrowheads*, image of the same section used for double labeling of AQP5 and NKAβ_1). (**C**) NKAβ_1-IR was present in all acinar cells, but the levels differed in a mosaic pattern: higher in some acinar cells and/or acini (*arrows*) than in others. NKAβ_1-IR in the ductal cells was uniformly high (*arrowheads*). (**D**) NHE1-IR was found at the basolateral membranes and within the cytoplasm of all acinar (*arrowhead*) and ductal cells, whereas the level in ductal cells was considerably higher (*arrows*). (**E**) NKCC1-IR was also present at the basolateral membranes and within the cytoplasm of all acinar (*arrowheads*) and ductal cells (*arrow*), but the levels were higher in the acinar cells. (**F**) CFTR-IR (*green*) was present in punctate aggregates within the apical cytoplasm of all acinar (*arrows*) and ductal cells (*arrowheads*), but the level in ductal cells was considerably higher. Rhodamine-conjugated phalloidin, which stains F-actin, was used to outline the morphologic profile (*red*, also in **G**). (**G**) ClC2γ. Like CFTR, ClC2γ-IR (*green*) was also found in the apical cytoplasm as punctate aggregates (*arrowheads*). However, no ClC2γ-IR was seen in ductal cells (*arrow*). Ac, acinus. Scale bar, 50 μm.

Downloaded from iovs.arvojournals.org on 04/23/2024

gland and have unique basal infoldings and numerous mitochondria, thus revealing the striations observed microscopically. This specialization greatly increases the membrane exchange area for the transport of ions and water. In predominantly serous salivary glands (parotid gland), the striated ducts are larger than in predominantly mucous glands (sublingual gland), a feature associated with the role of the striated duct in modifying isotonic basic saliva to produce hypotonic saliva. The absence of striated ducts in LGs may be because the lacrimal fluid is isotonic, rather than hypotonic, as in the case of saliva, and therefore there is no need to have these ducts. It appears that there are no distinctive morphologic features that distinguish one lacrimal duct segment from the other; rather, the cytological features change incrementally along the entire duct system.

Like other exocrine secretions, it is believed that lacrimal fluid is produced in two stages: formation of a primary fluid in the secretory end pieces, or acini, and modification into the final fluid during transit through the duct system. These two stages were confirmed some time ago by micropuncture analyses of lacrimal fluids from rat and rabbit.[8,20] The primary fluid resembles an isotonic ultrafiltrate of plasma at all flow rates. The final fluid has markedly different compositions depending on the flow rates, but generally a much higher $[K^+]$ and $[Cl^-]$ in rat, and a higher $[K^+]$ and similar $[Cl^-]$ in rabbit, both under basal conditions. Non–mutually exclusive explanations for this phenomenon are that duct cells secrete increased amounts of K^+ and Cl^- and that duct cells reabsorb Na^+ and Cl^-.

In an excellent study, Dartt et al.[21] reported electrolyte and water secretion in the rabbit lacrimal ducts. By using a microperfusion technique, they demonstrated that duct cells are actively involved in lacrimal secretion and that Na^+/K^+-ATPase may play a significant role. However, it was unclear from their report what duct segments were used for those studies, although it appears to have been intralobular ducts. Recent studies by Ubels et al. (*IOVS* 2005;46:ARVO E-Abstract 4424)[22] elegantly described the presence of transport proteins consistent with potassium secretion by ductal cells of rat LG and documented that approximately 150 genes are expressed at significantly higher levels in duct cells than in acinar cells. Although not explicitly stated, the micrographs in Ubels' papers appear to illustrate intra- and interlobular ducts. Another recent study found that lacrimal duct cells express functionally active NHE and AE, and parasympathomimetic stimulation by carbachol stimulates these two transporters through the elevation of intracellular $[Ca^{2+}]$, suggesting their role in ion and water regulation by duct cells.[23]

NKA is located in the plasma membranes of all animal cells, but preponderantly in the basal-lateral plasma membranes of the epithelia that comprise barriers between the interstitial fluid and the internal environment of the epithelial cells. Depending on the asymmetric localizations of other transport proteins, NKA may power net absorption or net secretion. It uses the energy released from hydrolysis of ATP to translocate Na^+ and K^+ ions across cell membranes. It moves Na^+ ions outwardly and K^+ inwardly, both against substantial electrochemical potential gradients. It is a heterotetramer composed of two α and two β subunits. So far, two α subunit isoforms (α1 and α2) and three β subunit isoforms (β1, β2, and β3) have been identified. Our real-time RT-PCR analyses detected transcripts for the α1, but not for the α2, subunit and for all three β subunits.

NKA has been localized in the basolateral membranes of lacrimal ductal epithelial cells, consistent with roles in both Na^+ reabsorption and K^+ secretion.[24] We have found no published determinations of the relative contribution the ducts make to the total volume of fluid secreted by the LG, although it has been estimated that the ducts account for roughly 30% of the final lacrimal fluid volume in physiological conditions.[25]

Net fluxes of anions and cations through co-transporters and exchangers are determined by mass action and ultimately by the transmembrane Na^+ concentration gradient that is established and maintained by NKA. Accordingly, NKCC mediate net fluxes of Na^+, K^+, and Cl^- into cells, and AE and NHE in concert mediate net fluxes of Na^+ and Cl^- into and net fluxes of H^+ and HCO_3^- out of cells. Whether the flux of Cl^- into an epithelium is in the absorptive or secretory direction depends on whether the transporters are localized in the apical or the basal-lateral plasma membrane.

The direction in which water flows across the plasma membranes is determined by osmotic gradients, which largely are established through the actions of various ion transport proteins such as just discussed. Aquaporins are the membrane proteins that are responsible for fast water transport across plasma membranes.[26–28] As we demonstrated here, in addition to acini, there are significant amounts of aquaporins in the ducts, suggesting their role in lacrimal secretion and/or reabsorption of luminal contents. The dramatic differences of mRNA transcripts in various duct segments also suggest that each duct segment plays different roles in lacrimal function.

The rabbit LG shares significant similarities with the human LG. As in humans, acinar lumens are ovoid in rabbit, whereas in mouse they are small and complexly folded with lumenal evaginations extending to the basal membrane (Schechter JE, et al. *IOVS* 2009;50:ARVO E-Abstract 3641).[18,29] Rabbits with dacryoadenitis also demonstrate many of the dry eye symptoms frequently observed in humans.[30] However, as in any animal model, there are also significant differences between human and rabbit tears (i.e., lipids secreted from the rabbit meibomian glands were the most different from human ones) (Butovich IA, et al. *IOVS* 2009;50:ARVO E-Abstract 2545). Nonetheless, the rabbit model has some unique advantages for LG studies and we believe data obtained from using these animals will help us to elucidate the mechanisms of the human LG.

In summary, the present studies established a nomenclature for the lacrimal duct system in the rabbit that was largely in accordance with that in the salivary glands, with the exception of the striated ducts. Our real-time RT-PCR data demonstrated that the lacrimal ducts are rich in mRNA of certain transporters and AQPs, and the mRNA abundance varied greatly among duct segments, suggesting that each segment plays a different role in lacrimal function. Immunofluorescence studies showed that immunoreactivity of AQPs and certain transporters was generally in accordance with the expression of various genes along the acinus-duct axis. The data provide evidence that lacrimal ducts are actively involved in LG fluid production and modification. Further studies are warranted to characterize transport proteins and their roles in LG function.

Acknowledgments

The authors thank Austin Mircheff and Joel Schechter for many helpful comments and discussions in experimental design and manuscript preparation; Deedar Samant and Padmaja Thomas for assistance with H&E staining; and Michele Mac Veigh for image analysis.

References

1. Hisada M, Botelho SY. Membrane potentials of in situ lacrimal gland in the cat. *Am J Physiol.* 1968;214:1262–1267.
2. Herzog V, Sies H, Miller F. Exocytosis in secretory cells of rat lacrimal gland: peroxidase release from lobules and isolated cells upon cholinergic stimulation. *J Cell Biol.* 1976;70:692–706.
3. Parod RJ, Putney JW. An alpha-adrenergic receptor mechanism controlling potassium permeability in the rat lacrimal gland acinar cell. *J Physiol.* 1978;281:359–369.
4. Raina S, Preston GM, Guggino WB, Agre P. Molecular cloning and characterization of an aquaporin cDNA from salivary, lacrimal, and respiratory tissues. *J Biol Chem.* 1995;270:1908–1912.

Downloaded from iovs.arvojournals.org on 04/23/2024

5. Hand A, Coleman R, Mazariegos MR, Lustmann J, Lotti LV. Endocytosis of proteins by salivary gland duct cells. *J Dent Res.* 1987; 66:412–419.
6. Ji Q, Chang L, Van Den Berg D, Stanczyk FZ, Stolz A. Selective reduction of AKR1C2 in prostate cancer and its role in DHT metabolism. *Prostate.* 2003;54:275–289.
7. Pflugfelder SC, Tseng SC, Sanabria O, et al. Evaluation of subjective assessments and objective diagnostic tests for diagnosing tear-film disorders known to cause ocular irritation. *Cornea.* 1998;17:38–56.
8. Alexander JH, van Lennep EW, Young JA. Water and electrolyte secretion by the exorbital lacrimal gland of the rat studied by micropuncture and catheterization techniques. *Pflugers Arch.* 1972;337:299–309.
9. Alexander JH, Young JA, van Lennep EW. The ultrastructure of the duct system in the rat exorbital lacrimal gland. *Z Zellforsch Mikrosk Anat.* 1973;144:453–466.
10. Kivela T. Antigenic profile of the human lacrimal gland. *J Histol Cytochem.* 1992;40:629–642.
11. Millar TJ, Herok G, Koutavas H, Martin DK, Anderton PJ. Immunohistochemical and histochemical characterization of epithelial cells of rabbit lacrimal glands in tissue sections and cell cultures. *Tissue Cell.* 1996;28:301–312.
12. Obata H, Yamamoto S, Horiuchi H, Machinami R. Histopathologic study of human lacrimal gland: statistical analysis with special reference to aging. *Ophthalmology.* 1995;102:678–686.
13. Obata H. Anatomy and histopathology of the human lacrimal gland. *Cornea.* 2006;25:S82–S89.
14. Ruskell GL. Nerve terminals and epithelial cell variety in the human lacrimal gland. *Cell Tissue Res.* 1975;158:121–136.
15. Sakai T. Major ocular glands (Harderian gland and lacrimal gland) of the musk shrew (Suncus murinus) with a review on the comparative anatomy and histology of the mammalian lacrimal glands. *J Morphol.* 1989;201:39–57.
16. Schechter JE, Carey J, Wallace M, Wood R. Distribution of growth factors and immune cells are altered in the lacrimal gland during pregnancy and lactation. *Exp Eye Res.* 2000;71:129–142.
17. Takashima Y, Takagi H, Takahashi M, et al. Endothelin protein expression in tear glands of the rabbit. *Curr Eye Res.* 1996;15: 768–773.
18. Walcott B. Anatomy and innervation of the human lacrimal gland. In: Albert DM, Jakobiec FA, eds. *Principles and Practice of Ophthalmology*. Philadelphia: Saunders Publishing; 1994;454–457.
19. Wieczorek R, Jakpbiec FA, Sacks EH, Knowles, DM. The immunoarchitecture of the normal human lacrimal gland: relevancy for understanding pathologic conditions. *Ophthalmology.* 1988:95: 100–109.
20. Rismondo V, Osgood TB, Leering P, Hattenhauer MG, Ubels JL, Edelhauser HF. Electrolyte composition of lacrimal gland fluid and tears of normal and vitamin A-deficient rabbits. *CLAO J.* 1989;15: 222–228.
21. Dartt DA, Moller M, Poulsen JH. Lacrimal gland electrolyte and water secretion in the rabbit: localization and role of (Na+ + K+)-activated ATPase. *J Physiol.* 1981;321:557–569.
22. Ubels JL, Hoffman HM, Srikanth S, Resau JH, Webb CP. Gene expression in rat lacrimal gland duct cells collected using laser capture microdissection: evidence for k+ secretion by duct cells. *Invest Ophthalmol Vis Sci.* 2006;47:1876–1885.
23. Tóth-Molnár E, Venglovecz V, Ozsvári B, et al. New experimental method to study acid/base transporters and their regulation in lacrimal gland ductal epithelia. *Invest Ophthalmol Vis Sci.* 2007; 48:3746–3755.
24. Bradley ME, Azuma KK, McDonough AA, Mircheff AK, Wood RL. Surface and intracellular pools of Na, K-ATPase catalytic and immuno-activities in rat exorbital lacrimal gland. *Exp Eye Res.* 1993; 57:403–413.
25. Mircheff AK. Water and electrolyte secretion and fluid modification. In: Albert DM, Jakobiec FA, eds. *Principles and Practice of Ophthalmology*. Philadelphia: WB Saunders; 1994;466–472.
26. Ishida N, Hirai SI, Mita S. Immunolocalization of aquaporin homologs in mouse lacrimal glands. *Biochem Biophys Res Commun.* 1997;238:891–895.
27. Hirai S, Ishida N, Watanabe K, Mita S. Leakage of aquaporin-5 in the tear of dacryoadenitis mice. *Invest Ophthalmol Vis Sci.* 2000;41: 2432–2437.
28. Tsubota K, Hirai S, King LS, Agre P, Ishida N. Defective cellular trafficking of lacrimal gland aquaporin-5 in Sjögren's syndrome. *Lancet.* 2001;357:688–689.
29. Ding C, Mac Veigh M, Pidgeon M, et al. Unique ultrastructure of lacrimal glands in NOD and BALB/c mice. *Curr Eye Res.* 2006;31: 13–22.
30. Zhu Z, Stevenson D, Schechter JE, Mircheff AK, Atkinson R, Trousdale MD. Lacrimal histopathology and ocular surface disease in a rabbit model of autoimmune dacryoadenitis. *Cornea.* 2003;22:25–32.

Downloaded from iovs.arvojournals.org on 04/23/2024